coatings

MDPI

Article

Finite Element Simulation of Stainless Steel Porous Scaffolds for Selective Laser Melting (SLM) and Its Experimental Investigation

Shubo Xu [1,*], Hailong Ma [1,*], Xiujuan Song [2], Sen Zhang [1], Xinzhi Hu [1] and Zixiang Meng [1]

[1] School of Materials Science and Engineering, Shandong Jianzhu University, Jinan 250101, China
[2] Jinan Engineering Polytechnic, Jinan 250200, China
* Correspondence: xsb@sdjzu.edu.cn (S.X.); mahailong@sdjzu.edu.cn (H.M.)

Abstract: In recent years, bone defect and bone tissue damage have become common clinical diseases. The development of bionic bone has had an important impact on the repair and reconstruction of bone tissue. Porous scaffolds have the advantages of adjustable pore size and controllable shape, which can solve the problem of mismatch in the process of bone repair, but traditional processing methods cannot overcome the challenge of the preparation of complex porous scaffolds. Therefore, 316L porous stainless steel scaffolds with different pore sizes (200 μm, 300 μm, 400 μm and 500 μm, respectively) were prepared by selective laser melting. Stress and strain were simulated and analyzed by using a finite element simulation method. Combined with a heat treatment experiment, a hardness test, a metallographic observation and a compression test, porous scaffolds were studied. The mechanical properties and microstructures of the scaffolds were studied and analyzed, and the optimized porous scaffolds were obtained. With reasonable melting parameters, the porous scaffolds that could meet the mechanical property requirements of load-bearing bone restorations were prepared by SLM.

Keywords: selective laser melting (SLM); finite element simulation; bionic bone; porous scaffolds

check for updates

Citation: Xu, S.; Ma, H.; Song, X.; Zhang, S.; Hu, X.; Meng, Z. Finite Element Simulation of Stainless Steel Porous Scaffolds for Selective Laser Melting (SLM) and Its Experimental Investigation. *Coatings* **2023**, *13*, 134. https://doi.org/10.3390/coatings13010134

Academic Editor: Bohayra Mortazavi

Received: 14 December 2022
Revised: 3 January 2023
Accepted: 4 January 2023
Published: 10 January 2023

Copyright: © 2023 by the authors. Licensee MDPI, Basel, Switzerland. This article is an open access article distributed under the terms and conditions of the Creative Commons Attribution (CC BY) license (https://creativecommons.org/licenses/by/4.0/).

1. Introduction

The use of 3D manufacturing technology produces 3D products by adding materials layer by layer [1–4] and is a kind of manufacturing method that is opposite to the traditional material removal processing method. By adding materials, and converting 3D CAD into STL facet files and other model data, we can directly manufacture a 3D physical entity model that is completely commensurate with the corresponding mathematical model. Because it does not need billets, it can realize the production and manufacture of products only by using the graphical data of a model made by a computer, can simplify the manufacturing procedure of products, shorten the development cycle of products, improve the production efficiency; it has been widely used in aerospace, automobile, motorcycle, household appliances, biomedicine, cultural creativity and other technological fields. It also has a unique position in engineering, scientific research, teaching and other fields of application. The laser-based powder bed fusion of metals (PBF-LB/M) [5] process is used in current Rapid Prototyping (RP)technology. PBF-LB/M is now considered to be a promising manufacturing technology, and we intend to apply it to orthopedic implants under load-bearing conditions [6]. Rehme et al. [7] studied and obtained the influence of laser parameters on the realization of microcrystalline lattice structures of various configurations. Figure 1 is the schematic diagram of the basic principles of SLM technology.

Why do we need to introduce biological concepts into additive manufacturing? How can people "copy" the ingenious and complex biological structures created by nature into industrial manufacturing? Increasingly, intelligent design software and 3D printing technology offer a shortcut to creating bionic structures [8]. Many of nature's materials are highly adaptable, while man-made materials are not. The density of steel material is higher

than other materials. Ceramic is fragile, while plastic is elastic. The parts made from these materials exhibit the properties of the source material throughout the process. On the other hand, many objects in nature exhibit adaptive density, elasticity, and brittleness in different areas for multiple purposes (e.g., combinations of muscles, veins, and bones) [9,10].

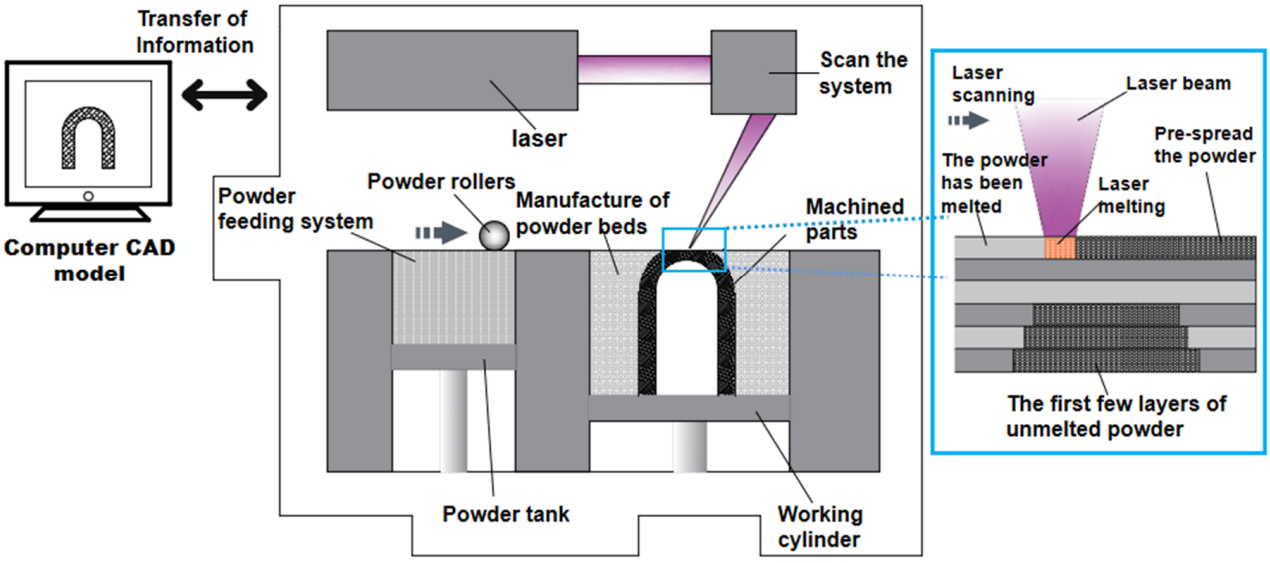


Figure 1. Schematic diagram of the basic principles of SLM technology.

In theory, most orthopedic surgeries now use standardized implants. Here, 3D printed personalized implants are mainly used to solve problems that cannot be solved by traditional surgery, as well as to meet high-end medical needs [11]. For example, in bone tumor repair surgery, personalized 3D-printed implants can meet the needs that cannot be met by traditional methods; this is a crucial demand for doctors and patients. As a new technology, 3D-printed personalized implants will coexist with traditional technologies fora long time. They will gradually replace traditional technologies after their long-term accumulation, on the basis of crucial-need cases [12,13]. The elastic modulus of stainless steel, titanium and titanium alloy is much higher than that of human bone, and it is easy to a produce "stress shielding" effect after implantation; this will affect the normal development of bone tissue near the implantation material [14]. Therefore, as a bone implant material, it is necessary to further improve the biological activity of stainless steel material to promote bone tissue regeneration [15–17]. Porous scaffolds also have the advantages of good penetration, adjustable pore size and porosity, and a similar elastic modulus to natural bone tissue, which can effectively prevent the generation of the stress shielding effect [16].

Natural bone tissue is a complex tissue with a precise porous structure. The ideal design of bone tissue engineering requires that the implant structure conforms to the anatomical structure of natural bone tissue [18]. In this paper, porous scaffolds for medical biology were prepared by SLM technology [19,20]. Porous scaffold is a promising bone graft, which provides a cell-friendly biological environment and simulates the bone structure [21]. This porous scaffold has good biocompatibility, bone tissue integration ability, good bone binding ability and appropriate mechanical properties [22]. The optimized porous scaffold not only replaces the damaged bone tissue, but also overcomes the shortcomings of the short-term implantation of porous scaffolds, manufactured by traditional technology. A 3D porous structure is conducive to cell adhesion, migration and proliferation, and provides the necessary living space for nutrition, metabolism and metabolic pathways to provide transport channels. Finally, implants and organisms are successfully integrated to achieve regeneration [23,24]. The homogenization calculations are of great significance for the study of porous composites [25–27].

Porous scaffolds have the advantages of adjustable pore size and controllable shape; this can solve the problem of mismatch in the process of bone repair, but traditional processing methods cannot overcome the challenge of preparing complex porous scaffolds. Therefore, 316L porous stainless steel scaffolds with different pore sizes (200 μm, 300 μm, 400 μm and 500 μm, respectively) were prepared by selective laser melting. Stress and strain were simulated and analyzed by the finite element simulation method. Combined with the heat treatment experiment, hardness test, metallographic observation and compression test, porous branches were studied. The mechanical properties and microstructures of the scaffolds were studied and analyzed, and the optimized porous scaffolds were obtained. With reasonable melting parameters, the porous scaffolds that could meet the mechanical property requirements of load-bearing bone restorations were prepared by SLM. The optimal porous scaffolds, obtained by the combination of finite element simulation and experimental analysis, can meet the mechanical property requirements of load-bearing bone prostheses.

2. Materials and Methods

2.1. Materials

Indeed, 316L Stainless Steel (SS) is one of the most commonly-used medical metal materials in the world [28]. It has the advantages of strong corrosion resistance, high strength, good processability and low cost. At present, 316L stainless steel is widely used in clinical medicine. It is widely used as human implant because of its excellent mechanical properties and good human compatibility. Because of the complex shape and the various sizes of artificial joints, traditional manufacturing technology has found it difficult to meet the market demand. SLM can produce porous scaffolds with complex shapes, and has been gradually applied in the field of biomedical sciences. Figure 2 shows the microscopic images of the morphology of 316L stainless steel powder, via scanning electron microscopy (ZEISS SUPRA 55, Mainz, Germany). It can be seen that 316L stainless steel powder has spherical distribution and the powder diameter is uniformly distributed around 40 μm. Table 1 shows the chemical composition of 316L Stainless Steel Powder (%). Table 2 gives the mechanical properties of 316L stainless steel (JIS G 4305-2005).

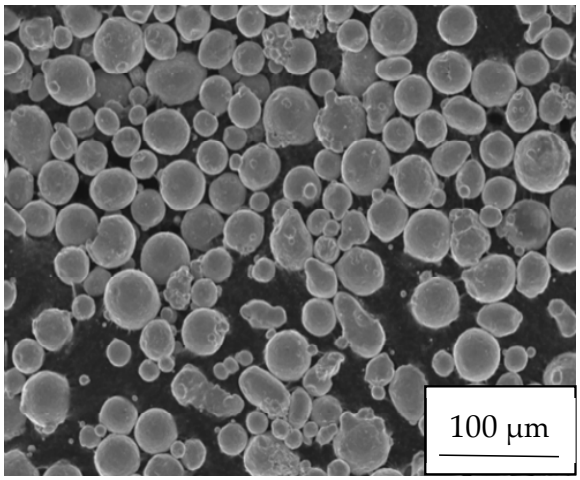


Figure 2. Morphology of 316L stainless steel powder.

Table 1. Chemical composition of 316L stainless steel powder (%).

Brand Name	C	Si	Mn	P	S	Ni	Cr	Mo
00Cr17Ni14Mo2	≤0.03	≤1.00	≤2.00	≤0.035	≤0.03	12.0–15.0	16.0–18.0	2.0–3.0

Table 2. Mechanical properties of 316L stainless steel (JIS G 4305-2005).

Distinguish	Ys Yield Strength (MPa)	Ts Tensile Strength (MPa)	El Elongation (%)	Hv Vickers Hardness	Remarks
Standard	≥205	≥520	≥40	≤200	2 B/1.5 t
SLM material	310	620	53	155	

2.2. Finite Element Models

The finite element analysis software (version 17.0) is ANSYS 17.0, and the porous scaffold model is modeled by SolidWoks software (version 2016). In order to ensure that the computational accuracy was improved while saving computational resources, the model cell mesh was divided using a tetrahedral mesh with a mesh size of 0.05 mm. The static mechanical model was a cylinder with a diameter of 10 mm and a height of 10 mm. The boundary conditions of the finite element model were consistent with the compression experiments, and the calculated load was an axial downward compression force of 3000 N. The boundary conditions at the bottom of the model were set to fully constrained. A large number of studies have shown that the ideal large hole size for bone tissue engineering is approximately 300–900 μm, and the porosity is between 60% and 95%. Considering that the optimal size range of bone growth and angiogenesis is 100–500 μm, the internal structure of the scaffold selected in this paper is connected to pore structure, and the pore size is set as 200 μm, 300 μm, 400 μm, and 500 μm, respectively. In the simulation, the elastic modulus of the stainless steel material E is selected as 196 GPa, and Poisson's ratio ν is selected as 0.3.

2.3. Manufacture of Porous Scaffolds

In this study, a laser power of 150 W, a scanning spacing of 0.06 mm, a scanning speed of 500 mm/s and a powder layer thickness of 0.035 mm were selected to construct a porous bone scaffold. Figure 3 shows the solid model of the 3D implant scaffolds with different apertures. The complex 3D model of porous scaffolds with different apertures was constructed by using Soildworks software. Figure 3a has a porosity of 200 μm, Figure 3b has a porosity of 300 μm, Figure 3c has a porosity of 400 μm, and Figure 3d has a porosity of 500 μm. Figure 4 shows 316L stainless steel porous scaffolds with different pore diameters, formed by SLM.The porous solid 316L stainless steel implant scaffold was prepared by melting metal powder with SLM technology. The pore diameter of the scaffold increased from 0 μm, 200 μm, 300 μm, 400 μm and 500 μm, respectively.

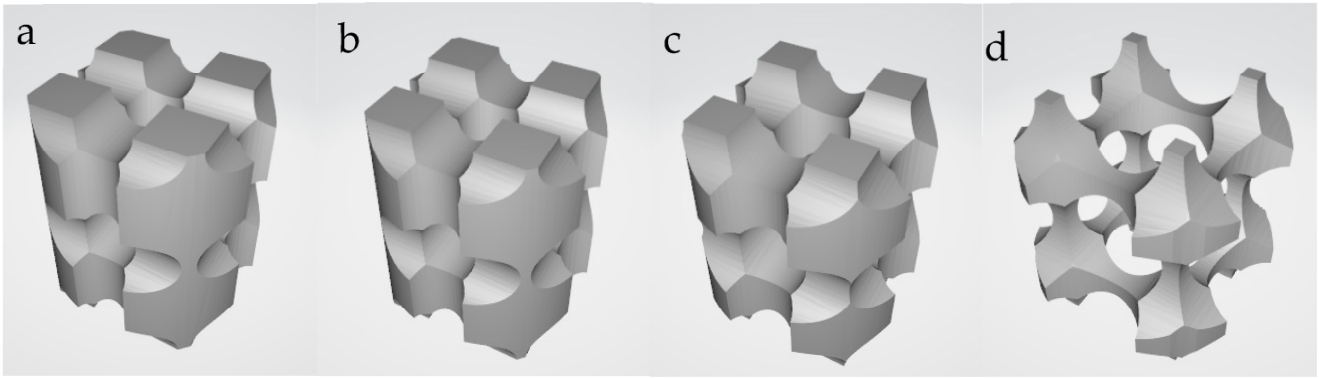


Figure 3. Three-dimensional solid models of implants with different apertures; (**a**) is 200 μm, (**b**) is 300 μm, (**c**) is 400 μm, and (**d**) is 500 μm.

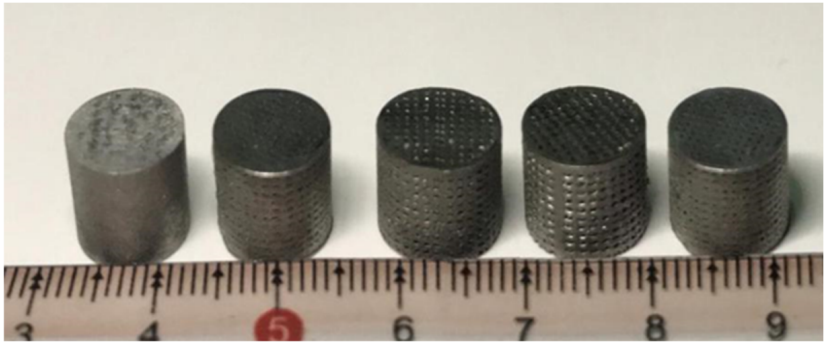


Figure 4. The 316L stainless steel porous scaffolds with different pore diameters, formed byusing SLM.

3. Results and Discussion

3.1. Finite Element Analysis

A large number of studies have shown that the ideal macro-pore size for bone tissue engineering is approximately 300–900 μm, and the porosity is between 60% and 95% [28–30]. Considering that the optimum size range of bone growth and angiogenesis is 100–500 μm, the internal structure of the scaffold selected in this paper is connected to pore structure. The aperture sizes are set to 200 μm, 300 μm, 400 μm and 500 μm, respectively. The porous metal parts ensure the biomechanical properties of the bone restorations. They have good corrosion resistance, wear resistance and mechanical properties [31]. They are especially suitable for the manufacture of artificial restorations. As the porous structure is applied to human bones, the stress of human bones is mainly compressive stress; therefore, this paper mainly conducts compression test experiments on the porous structure test pieces, and takes experimental data and simulation results as analysis objects. However, due to the complexity of the porous structure in this study, the finite element mechanical numerical simulation analysis of the porous structure is only limited to the range of linear elastic deformation, and its force direction is shown in Figure 5.

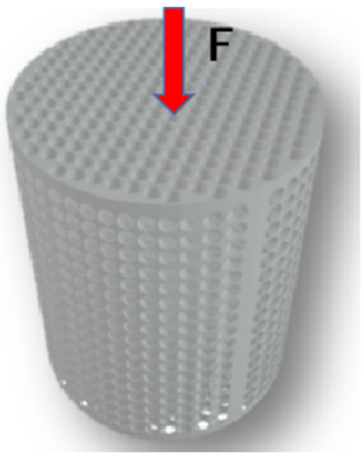


Figure 5. The force model of porous structure in finite element compression simulation. (red arrow is direction of force and F is force).

3.2. Simulation Numerical Results Discussion

The stress–strain analysis of porous scaffolds with different pore sizes was performed by using finite element simulation analysis, and the optimized scaffold porosity structure was obtained. Figure 6 shows the deformation, stress and strain nephograms of porous scaffolds with different pore sizes, and the ends of the porous scaffolds were compressed unilaterally. From Figure 6a–d, it can be seen that the deformation at the upper end of the specimens is higher than the other part of specimen, and that the deformation limit of the

scaffold was higher than that of deformation limit of natural bone. For the stress distribution of scaffolds, it can be seen from Figure 6e–h that the stress at the upper and bottom of the scaffolds is higher at the beginning stage. With the deformation proceeding, under the condition that the porosity of the porous scaffolds is similar, the stress distribution can be obtained from the stress-deformation nephogram of the scaffolds. The porous scaffolds with a diameter of 300 μm can effectively relieve the local stress concentration. Figure 6i–l support position, using the principle of equidistant points, and its strain, is plotted as shown in Figure 7. It can be seen that, with the increase in porosity, the effective strain presents a gradient rise.

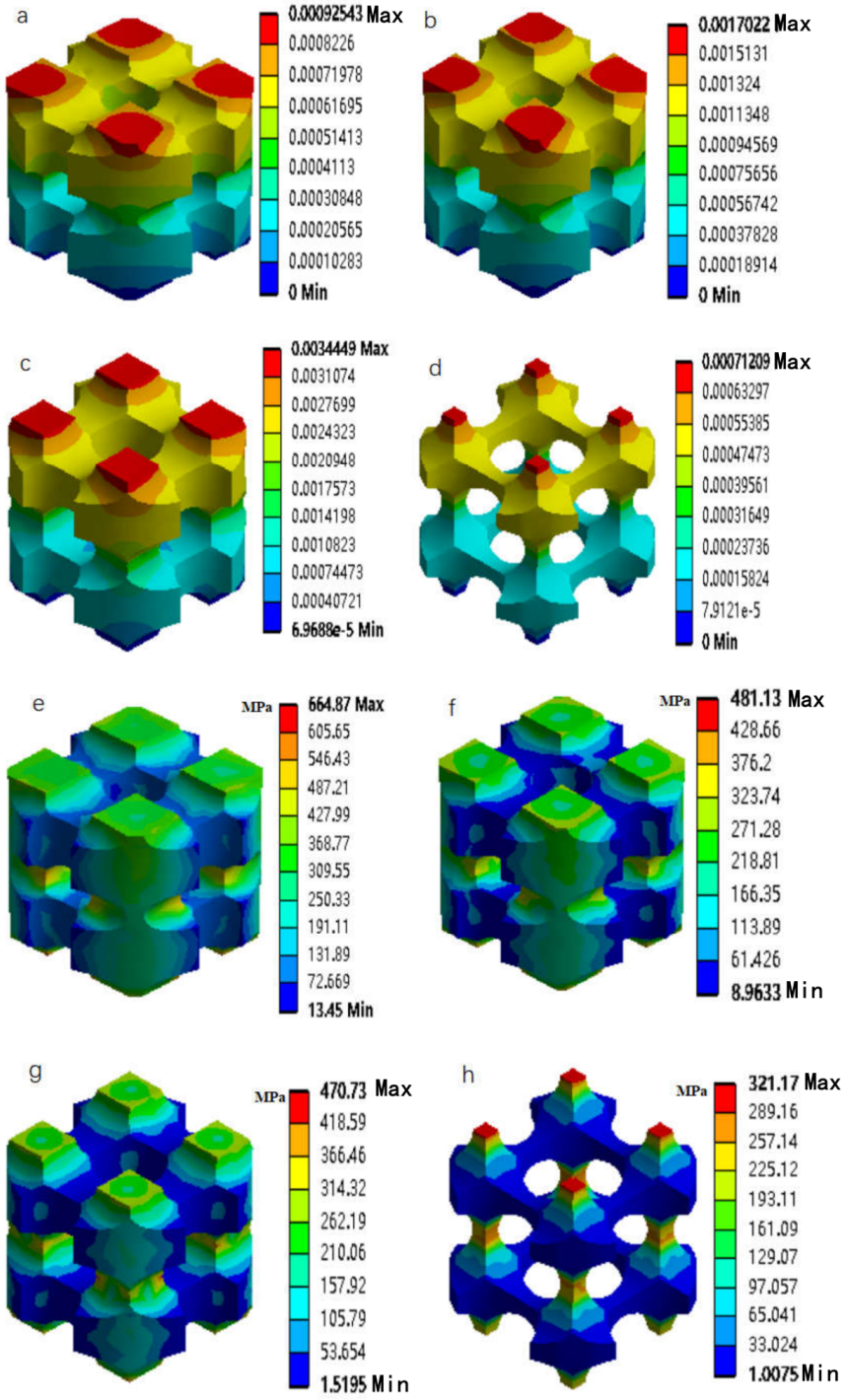


Figure 6. *Cont.*

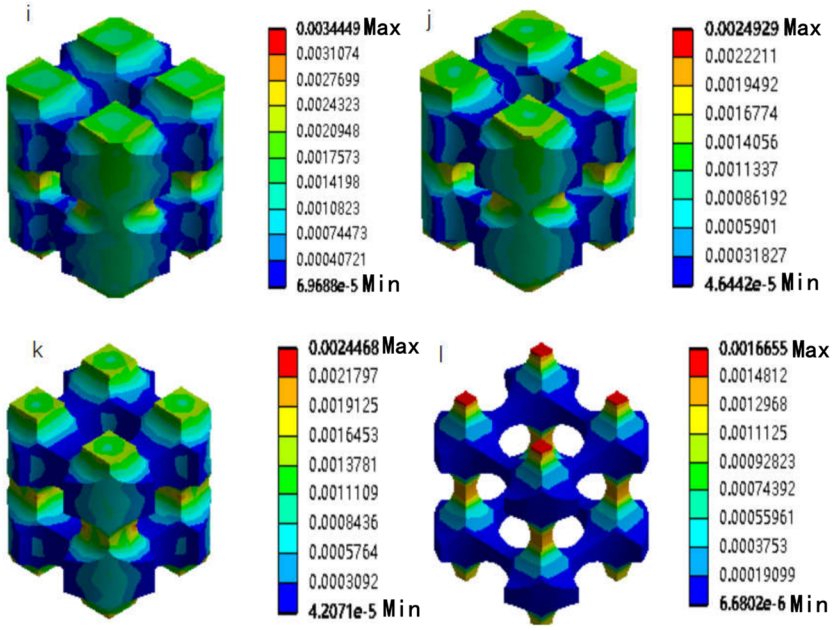


Figure 6. Total deformation nephogram of porous scaffolds with aperture size of 200 μm, 300 μm, 400 μm and 500 μm, respectively (**a**–**d**), Stress analysis nephograms of porous scaffolds with aperture sizes of 200 μm, 300 μm, 400 μm and 500 μm (**e**–**h**), Strain analysis nephograms of porous scaffolds with aperture sizes of 200 μm, 300 μm, 400 μm and 500 μm (**i**–**l**).

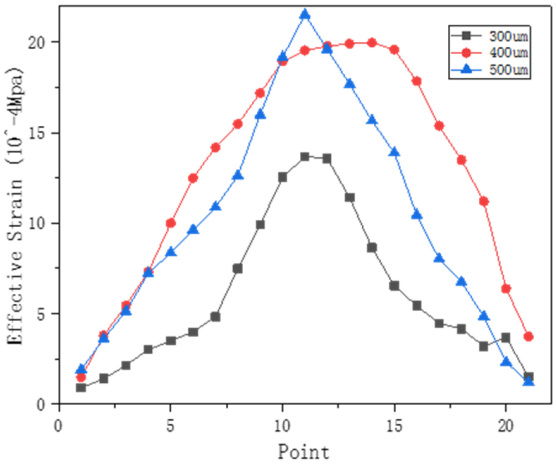


Figure 7. Equivalent strain distribution of scaffolds with different diameters.

The numerical simulation of the selective laser melting of porous scaffolds with different apertures was carried out by finite element analysis. Selective laser melting was carried out under the same conditions. The average elastic modulus of the scaffolds with different apertures was obtained, as shown in Table 3. The elastic modulus of human bone with a higher transplantation rate ranges from 10 to 30 GPa [32]. On the one hand, the design of scaffolds is to obtain a high-strength structure; on the other hand, it is also a process to obtain a perfect match between the mechanical properties of the scaffold and the surrounding bone tissue. If the elastic modulus of the scaffold exceeds the elastic modulus of the natural bone after implantation, it is easy to produce a stress shielding phenomenon; this causes osteoporosis around the implanted bone tissue and easily leads to fracture. Therefore, it can be concluded from the above analysis that among the porous scaffolds, the one with the pore size of 300 μm can withstand the greatest pressure, and the one with the pore size of 300 μm is more suitable for the load-bearing role of the human bone implant.

Table 3. Compressive strength and elastic modulus of different apertures.

Aperture Size (μm)	Compressive Strength/MPa	Modulus of Elasticity (GPa)
300	514	10.38
400	488	6.38
500	465	5.56

3.3. Compression Experimental Analysis

The porous scaffolds with an aperture size of 200 μm, 300 μm, 400 μm and 500 μm, respectively, were subjected to compression tests. Their test loads were 28.4 KN, 51.9 KN, 25.5 KN and 23.8 KN in turn. It can be seen that the strength of the scaffold model is the best when the aperture is 300 μm. Figure 8 shows the curves of the test force and the deformation obtained from the compression tests of the scaffolds with different diameters. In the case of the same deformation, the porous scaffolds with the diameter of 300 μm can bear the greatest test force (in addition to solid scaffolds).It can be concluded that the pressure-bearing capacity of porous scaffolds with an aperture size of 300 μm is higher than that of porous scaffolds with an aperture size of 400 μm and 500 μm, respectively.

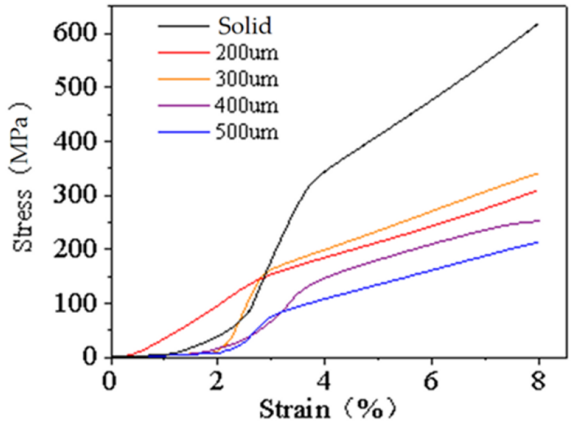


Figure 8. Stress–strain curves of scaffolds with different diameters.

3.4. Microstructure Analysis

All Scaffolds are uniformly manufactured under the same conditions, with regular holes. Figure 9 gives the optical and SEM morphology of the porous scaffolds. From Figure 9, it can be seen that the prepared porous scaffolds have a compact and uniform structure, without defects. In an observation from Figure 9(A1–A4), SLM forms a porous scaffold surface and there is uniform melting. It can be seen that the pore shape is basically circular, there is no obvious crack, the forming quality is relatively complete, and there is no over-melting phenomenon. The scaffold has a well-connected macroporous structure, many micro-spheres are observed on the wall surface of the scaffold frame gap, and the size range of micro-spheres is 30–50 μm. The scaffold pore hole shown in the picture does contain some non-melting or adhesive globular particles. The spheroidization of SLM can be observed from the SEM image of the scaffold in Figure 9(B1–B4). Metal powders are melted via selective laser melting. It can be seen from the figure that the prepared porous scaffold has a dense and uniform structure, and that the forming part is mainly composed of columnar crystals with the same growth direction. The columnar crystal arrangement has the same directionality and uniform distribution, and the periphery is densely distributed with fine equiaxed crystals. Due to the high temperature and high gradient solidification characteristics of the rapid molding technology, the resulting structure is fine, uniform, and the microstructure is arranged regularly.

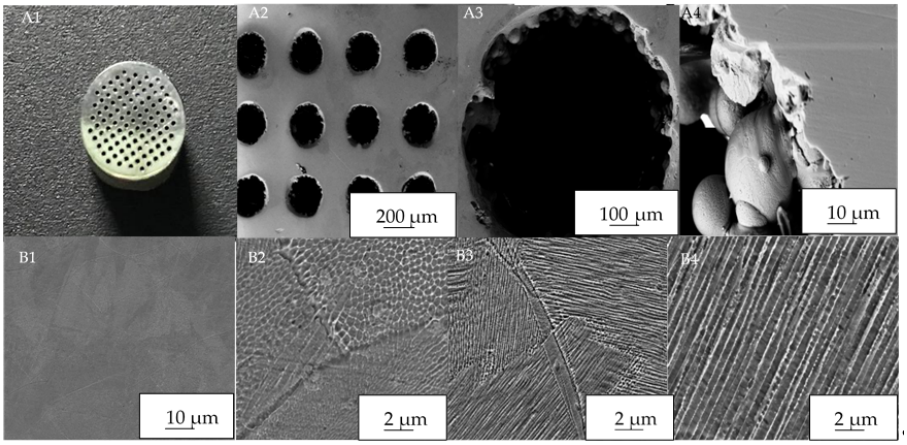


Figure 9. (**A1**) Optical morphology and porous scaffolds: (**A2**–**A4**) Representational SEM images of porous scaffolds at different magnifications. Microstructure photographs of porous scaffolds under SEM: (**B1**–**B4**) Microstructure photographs at different magnifications.

3.5. Experimental Analysis of Heat Treatment

Because SLM-forming technology involves a complex metallurgical process, including metal powder through high-speed laser scanning, instantaneous melting, solidification, the cooling process, and the process forming workpieces, extensive residual stress is produced; however, bubbles and poor sintering defects are also produced, which not only affect the microstructure of the porous scaffolds, but also affect the mechanical properties of the materials.

In this paper, the method of heat treatment is used to improve the mechanical properties of materials and eliminate the participating stress. Stress relief annealing is used to heat the temperature below the phase transformation temperature, and then cool it slowly in the air. Therefore, no structural transformation occurs during the heat treatment process. This experiment adopted a heat treatment process with a heating temperature of 800 °C, heat preservation of 100 min and furnace cooling. The hardness values of supports with different pore sizes, before and after heat treatment, were found. The hardness was measured by a Vickers hardness tester, the test load was 1000 N, each sample was measured five times, and the average value was taken. Table 4 shows the Vickers hardness changes in four different structure scaffolds, before and after heat treatment. The experimental results show that the heat treatment method can reduce the hardness of the scaffold well and match the mechanical properties of human bone.

Table 4. Hardness change before and after heat treatment.

Aperture Size (μm)	Before Heat Treatment (HV)	After Heat Treatment (HV)
300	276	224
400	268	224
500	262	220
Solid	258	220

4. Conclusions

The porous scaffolds with different pore sizes, prepared by SLM, have great potential to replace bone tissue and precisely control porosity and pore size. Through the combination of finite element simulation analysis and experimental study, the scaffold model with the most suitable mechanical properties—porous scaffolds and different pore sizes—was obtained, and the mechanical properties of human bone tissue were better matched through heat treatment. The main conclusions are as follows:

(1) The deformation at the upper end of the specimens is higher, and the deformation limit of the scaffold is higher than that of deformation limit of natural bone. The

porous scaffolds with a diameter of 300 μm can effectively relieve the local stress concentration. With the increase in porosity, the effective strain presents a gradient rise. In addition, the one with the pore size of 300 μm is more suitable for the load-bearing role of the human bone implant.

(2) The prepared porous scaffold has a dense and uniform structure, and the forming part is mainly composed of columnar crystals with the same growth direction. The columnar crystal arrangement has the same directionality and uniform distribution, and the periphery is densely distributed with fine equiaxed crystals. Due to the high temperature and high gradient solidification characteristics of the rapid molding technology, the resulting structure is fine, uniform, and the microstructure is arranged regularly.

(3) Through finite element simulation analysis, the reasonable pore diameter of the porous scaffold is obtained, and the optimized pore size of the porous scaffold is obtained. The elastic modulus of the porous scaffold with a pore size of 300 μm isclosest to the elastic modulus required by human bone. Therefore, the comprehensive mechanical properties of the scaffold with the pore size of 300 μm arethe best match with that of human bone. The identification of the porous scaffold that is more suitable for the load-bearing effects of human bone can guide the follow-up research.

Author Contributions: Conceptualization, H.M.; Methodology, S.X., H.M. and X.S.; Software, S.Z. and X.H.; Formal analysis, S.X.; Data curation, S.X. and X.S.; Writing—original draft, Z.M.; Writing—review & editing, H.M.; Funding acquisition, S.X. All authors have read and agreed to the published version of the manuscript.

Funding: The study was supported by Natural Science Foundation of Shandong Province, China (ZR2021ME182 and ZR2021JL017), National College Student Innovation and Entrepreneurship Program (S20211043001, 202210430010 and 202210430008), the Science and Technology Enterprise Innovation Program of Shandong Province, China (2022TSGC2108 and 2022TSGC2402), the Shandong Graduate Education and Teaching Reform Research Project (Grant No. SDYJG21169) and the High quality curriculum construction project of Shandong Jianzhu University graduate education (YZKC202210 and ALK202210).

Institutional Review Board Statement: Not applicable.

Informed Consent Statement: Not applicable.

Data Availability Statement: Not applicable.

Conflicts of Interest: The authors declare no conflict of interest.

References

1. Huan, Z.J.; Chu, H.K.; Liu, H.B.; Yang, J.; Sun, D. Engineered bone scaffolds with Dielectrophoresis-based patterning using 3D printing. *Biomed. Microdevices* **2017**, *19*, 102. [CrossRef] [PubMed]
2. Huang, B.Y.; Bartlo, P.J. Rheological characterization of polymer/ceramic blends for 3D printing of bone scaffolds. *Polym. Test.* **2018**, *68*, 365. [CrossRef]
3. Tan, X.P.; Tan, Y.J.; Chow, C.S.L.; Tor, S.B.; Yeong, W.Y. Metallic powder-bed based 3D printing of cellular scaffolds for orthopaedic implants: A state-of-the-art review on manufacturing, topological design, mechanical properties and biocompatibility. *Mater. Sci. Eng. C* **2017**, *76*, 1328–1343. [CrossRef] [PubMed]
4. Henriques, B.; Pinto, P.; Silva, F.S.; Fredel, M.C.; Fabris, D.; Souza, J.C.M.; Carvalho, O. On the mechanical properties of monolithic and laminated nano-ceramic resin structures obtained by laser printing. *Compos. Part B Eng.* **2018**, *141*, 76–83. [CrossRef]
5. Gülcan, O.; Simsek, U.; Cokgunlu, O.; Özdemir, M.; Şendur, P.; Yapici, G.G. Effect of Build Parameters on the Compressive Behavior of Additive Manufactured CoCrMo Lattice Parts Based on Experimental Design. *Metals* **2022**, *12*, 1104. [CrossRef]
6. Chen, Z.; Yan, X.; Yin, S.; Liu, L.; Liu, X.; Zhao, G.; Ma, W.; Qi, W.; Ren, Z.; Liao, H.; et al. Influence of the pore size and porosity of selective laser melted Ti6Al4V ELI porous scaffold on cell proliferation, osteogenesis and bone ingrowth. *Mater. Sci. Eng. C* **2019**, *106*, 110289. [CrossRef] [PubMed]
7. Tsopanos, S.; Mines, R.A.W.; Mckown, S.; Shen, Y.; Cantwell, W.J.; Brooks, W.; Sutcliffe, C.J. The Influence of Processing Parameters on the Mechanical Properties of Selectively Laser Melted Stainless Steel Microlattice Structures. *J. Manuf. Sci. Eng.* **2010**, *132*, 041011. [CrossRef]
8. Li, L.; Shi, J.; Zhang, K.; Yang, L.; Yu, F.; Zhu, L.; Liang, H.; Wang, X.; Jiang, Q. Early osteointegration evaluation of porous Ti6Al4V scaffolds designed based on triply periodic minimal surface models. *J. Orthop. Transl.* **2019**, *19*, 94–105. [CrossRef]

9. Ouyang, P.; Dong, H.; He, X.; Cai, X.; Wang, Y.; Li, J.; Li, H.; Jin, Z. Hydromechanical mechanism behind the effect of pore size of porous titanium scaffolds on osteoblast response and bone ingrowth. *Mater. Des.* **2019**, *183*, 108151. [CrossRef]
10. Wang, L.; Kang, J.; Sun, C.; Li, D.; Cao, Y.; Jin, Z. Mapping porous microstructures to yield desired mechanical properties for application in 3D printed bone scaffolds and orthopaedic implants. *Mater. Des.* **2017**, *133*, 62–68. [CrossRef]
11. Cuadrado, A.; Yánez, A.; Martel, O.; Deviaene, S.; Monopoli, D. Influence of load orientation and of types of loads on the mechanical properties of porous Ti6Al4V biomaterials. *Mater. Des.* **2017**, *135*, 309–318. [CrossRef]
12. Arjunan, A.; Demetriou, M.; Baroutaji, A.; Wang, C. Mechanical performance of highly permeable laser melted Ti6Al4V bone scaffolds. *J. Mech. Behav. Biomed. Mater.* **2019**, *102*, 103517. [CrossRef]
13. Rüdrich, U.; Lasgorceix, M.; Champion, E.; Pascaud-Mathieu, P.; Damia, C.; Chartier, T.; Brie, J.; Magnaudeix, A. Pre-osteoblast cell colonization of porous silicon substituted hydroxyapatite bioceramics: Influence of microporosity and macropore design. *Mater. Sci. Eng. C* **2019**, *97*, 510–528. [CrossRef]
14. Van Bael, S.; Chai, Y.C.; Truscello, S.; Moesen, M.; Kerckhofs, G.; Van Oosterwyck, H.; Kruth, J.-P.; Schrooten, J. The effect of pore geometry on the in vitro biological behavior of human periosteum-derived cells seeded on selective laser-melted Ti6Al4V bone scaffolds. *Acta Biomater.* **2012**, *8*, 2824–2834. [CrossRef]
15. Ma, M.; Wang, Z.; Wang, D.; Zeng, X. Control of shape and performance for direct laser fabrication of precision large-scale metal parts with 316L Stainless Steel. *Opt. Laser Technol.* **2013**, *45*, 209–216. [CrossRef]
16. Jiang, H.-Z.; Li, Z.-Y.; Feng, T.; Wu, P.-Y.; Chen, Q.-S.; Feng, Y.-L.; Chen, L.-F.; Hou, J.-Y.; Xu, H.-J. Effect of Process Parameters on Defects, Melt Pool Shape, Microstructure, and Tensile Behavior of 316L Stainless Steel Produced by Selective Laser Melting. *Acta Metall. Sin. Engl. Lett.* **2020**, *34*, 495–510. [CrossRef]
17. Zhang, J.W.; Xiao, D.Q.; He, X.; Shi, F.; Luo, P.F.; Zhi, W.; Duan, K.; Weng, J. A novel porous bioceramic scaffold by accumulating hydroxyapatite spheres for large bone tissue engineering. III: Characterization of porous structure. *Mater. Sci. Eng. C* **2018**, *89*, 223. [CrossRef]
18. Yao, Q.Q.; Liu, Y.X.; Selvaratnam, B.; Koodali, R.T.; Sun, H.L. Mesoporous silicate nano-particles/3D nanofibrous scaffold-mediated dual-drug delivery for bone tissue en-gineering. *J. Control. Release* **2018**, *279*, 69. [CrossRef]
19. Tang, Q.G.; Piard, C.; Lin, J.; Nan, K.; Guo, T.; Caccamese, J.; Fisher, J.; Chen, Y. Imaging stem cell dis-tribution, growth, migration, and differentiation in 3-D scaffolds for bone tissue engineering using mesoscopic fluorescence tomography. *Biotechnol. Bioeng.* **2018**, *115*, 257. [CrossRef]
20. Wu, S.Y.; Wang, J.D.; Zou, L.Y.; Jin, L.; Wang, Z.L.; Li, Y. A three-dimensional hydro-xyapatite/polyacrylonitrile composite scaffold designed for bone tissue engineering. *RSC Adv.* **2018**, *8*, 1730–1736. [CrossRef]
21. Xie, X.; Wang, X.; Yao, D.; Hung, L.; Qin, L. Imparied bone healing in rabbits with steroid-induced osteonecrosis. *J. Bone Jt. Surg.* **2011**, *93*, 558. [CrossRef] [PubMed]
22. Sharma, A.; Molla, S.; Katti, K.S.; Katti, D.R. Multiscale models of degradation and healing of bone tissue engineering nanocomposite scaffolds. *J. Nanomech. Micr.* **2017**, *7*, 4. [CrossRef]
23. Yan, Y.; Kang, Y.J.; Li, D.; Yu, K.; Xiao, T.; Wang, Q.Y.; Deng, Y.; Fang, H.; Jiang, D.; Zhang, Y. Microstructure, mechanical properties and corrosion behavior of porous Mg-6 wt.% Zn scaffolds for bone tissue engineering. *J. Mater. Eng. Perform.* **2018**, *27*, 970. [CrossRef]
24. Coffigniez, M.; Gremillard, L.; Balvay, S.; Lachambre, J.; Adrien, J.; Boulnat, X. Direct-ink writing of strong and biocompatible titanium scaffolds with bimodal interconnected porosity. *Addit. Manuf.* **2021**, *39*, 101859. [CrossRef]
25. Shahzamanian, M.M.; Shahrjerdi, A.; Sahari, B.B.; Wu, P.D. Steady-State Thermal Analysis of Functionally Graded Rotating Disks Using Finite Element and Analytical Methods. *Materials* **2022**, *15*, 5548. [CrossRef] [PubMed]
26. Shahzamanian, M.M.; Thomsen, C.; Partovi, A.; Xu, Z.T.; Wu, P.D. The effect of superimposed hydrostatic pressure on shear decohesion in round bar tensile specimens. *Int. J. Fracture* **2022**, *233*, 179–194. [CrossRef]
27. Shahzamanian, M.M.; Thomsen, C.; Partovi, A.; Xu, Z.T.; Wu, P.D. Numerical Study about the Influence of Superimposed Hydrostatic Pressure on Shear Damage Mechanism in Sheet Metals. *Metals* **2021**, *11*, 1193. [CrossRef]
28. Zhang, S.; Xu, S.; Pan, Y.; Li, J.; Li, T. Mechanism Study of the Effect of Selective Laser Melting Energy Density on the Microstructure and Properties of Formed Renewable Porous Bone Scaffolds. *Metals* **2022**, *12*, 1712. [CrossRef]
29. Zhang, K.; Fan, Y.B.; Dunne, N.; Li, X.M. Effect of microporosity on scaffolds for bone tissue engineering. *Regen. Biomater.* **2018**, *5*, 115. [CrossRef]
30. Arabi, N.; Zamanian, A.; Rashvand, S.N.; Ghorbani, F. The tunable porous structure of gelatin-bioglass nanocomposite scaffolds for bone tissue engineering applications: Physicochemical, mechanical, and in vitro properties. *Macromol. Mater. Eng.* **2018**, *303*, 1700539. [CrossRef]
31. Arahira, T.; Maruta, M.; Matsuya, S.; Todo, M. Development and characterization of a novel porous beta-TCP scaffold with a three-dimensional PLLA network structure for use in bone tissue engineering. *Mater. Lett.* **2015**, *152*, 148. [CrossRef]
32. Xu, S.; Zhang, S.; Ren, G.; Pan, Y.; Li, J. Optimization of Structural and Processing Parameters for Selective Laser Melting of Porous 316L Bone Scaffolds. *Materials* **2022**, *15*, 5896. [CrossRef] [PubMed]

Disclaimer/Publisher's Note: The statements, opinions and data contained in all publications are solely those of the individual author(s) and contributor(s) and not of MDPI and/or the editor(s). MDPI and/or the editor(s) disclaim responsibility for any injury to people or property resulting from any ideas, methods, instructions or products referred to in the content.